nature cell biology

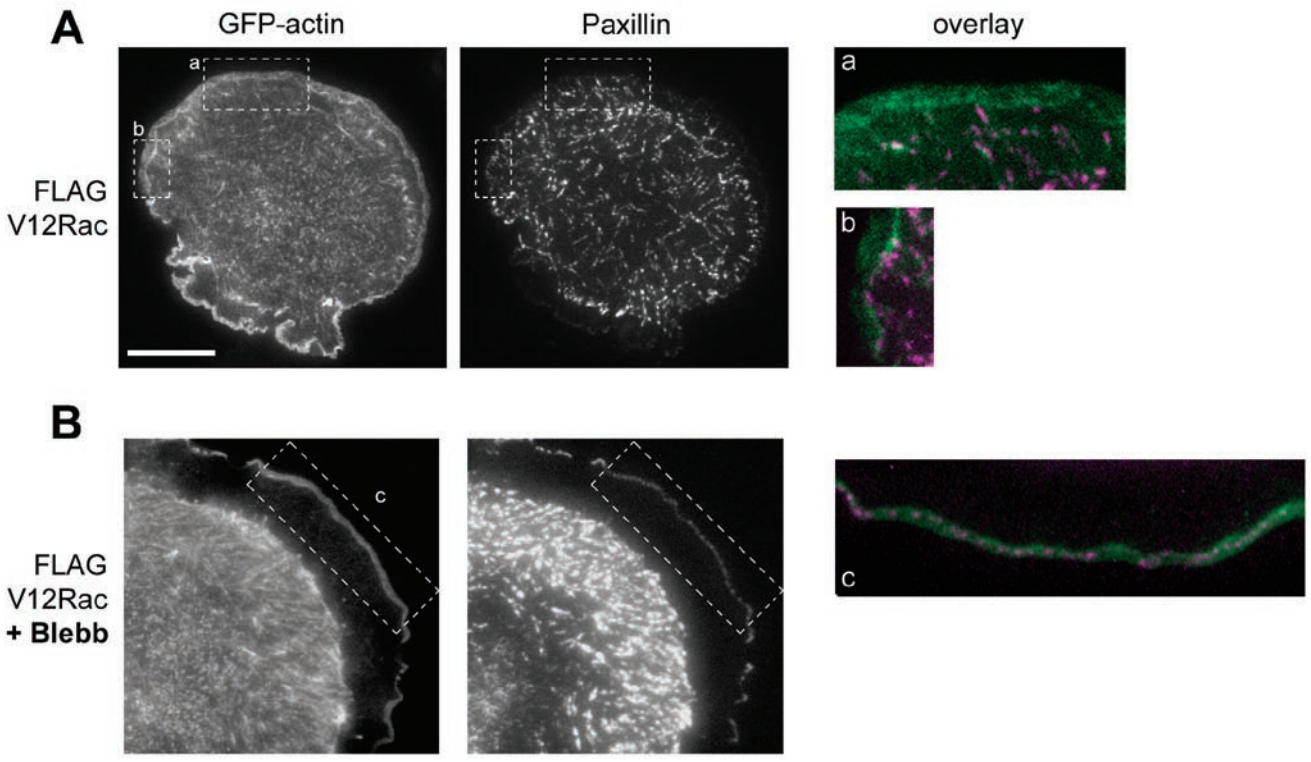

Figure S1 Activated Rac induced focal complexes differ from nascent adhesions. CHO.K1 cells expressing V12Rac, either without (A) or with 20 μM blebbistatin (B), were co-transfected with GFP-actin (left) and paxillin-mOrange (right). Scale bar = 10 μm. Color inserts show the relative positioning of paxillin-containing focal complexes (A) or nascent adhesions (B) with respect to the lamellipodium. Green, actin; magenta, paxillin. Note that the focal complexes reside the lamellipodium-lamellum interface and disassemble into smaller, lamellipodial localized nascent-like adhesions the presence of blebbistatin.

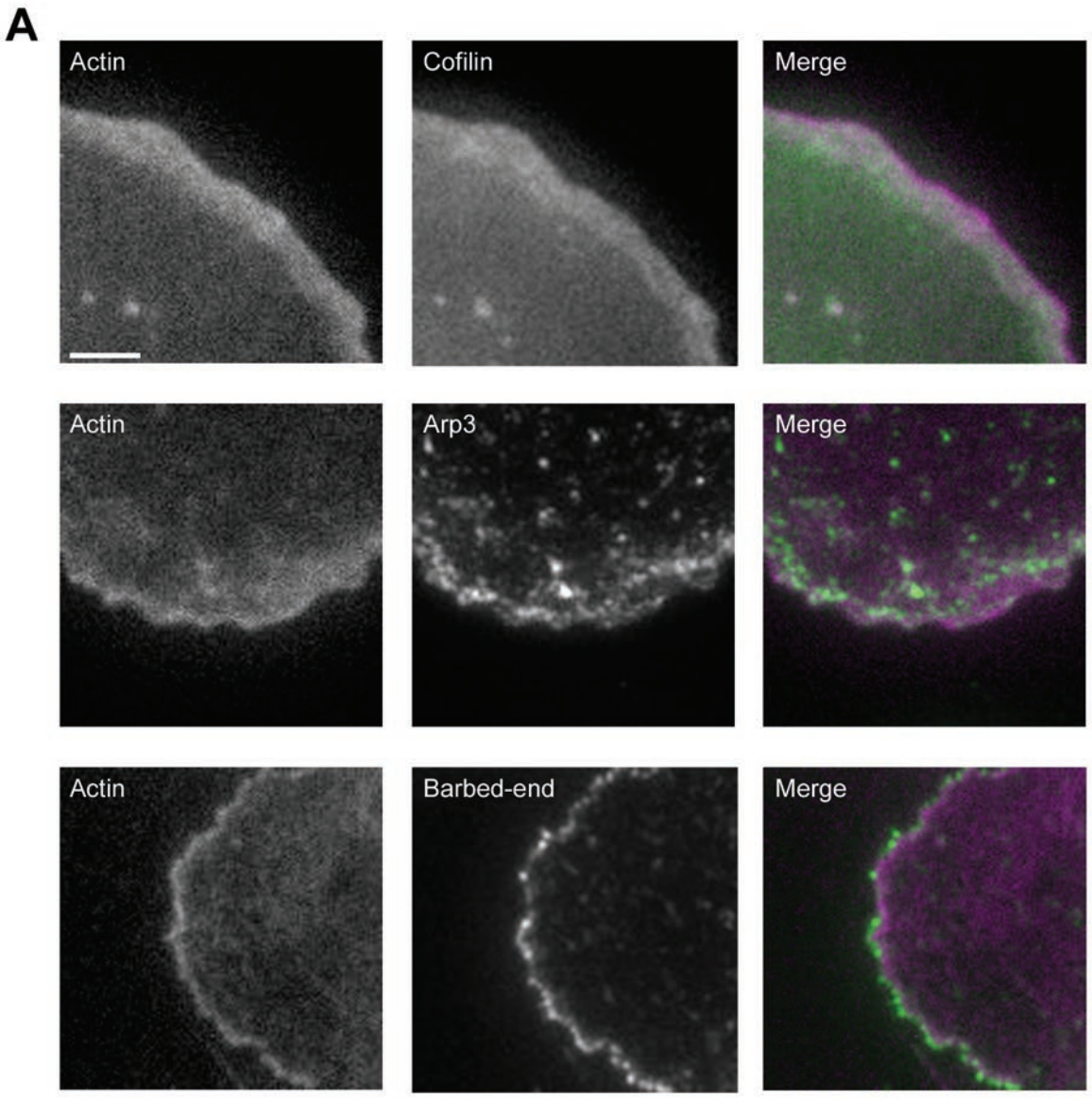

Figure S2 Molecular markers of the lamellipodium of migrating CHO.K1 cells. Characterization of dendritic actin of the lamellipodia. mRFP-actin (magenta) colocalize with GFP-cofilin and immunostaining of Arp3 (green). Barbed-end actin (green) outlines fluorescent phalloidin (magenta) at the leading edge.

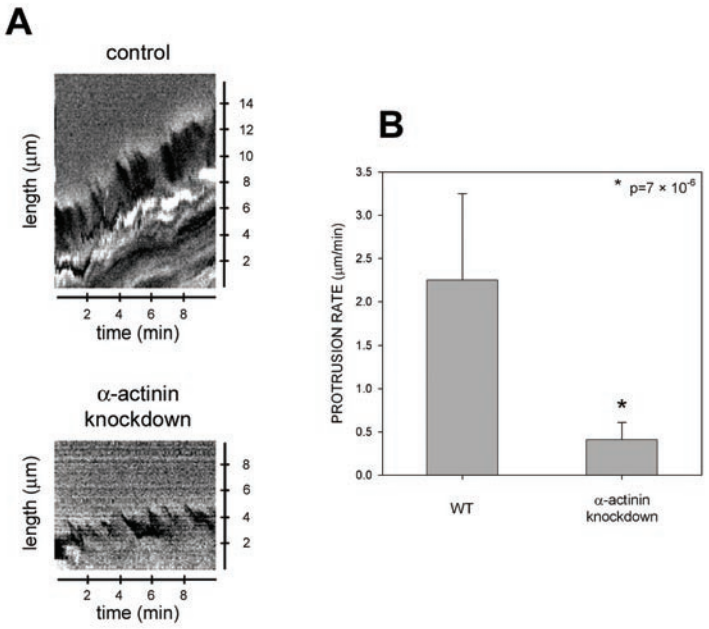

Figure S3 Quantification of protrusion rates in α-actinin-knockdown cells. (A) Kymographs from control (pSUPER) and α-actinin-depleted cells. The knockdown cells were identified by coexpression of a GFP marker, imaged in brightfield, and then analyzed by kymography. (B) Quantification of protrusion rates from kymographs from (A). Average protrusion rates measured from >12 cells (three to five protrusions/cell) from four independent experiments. Error bars represent ±SEM.

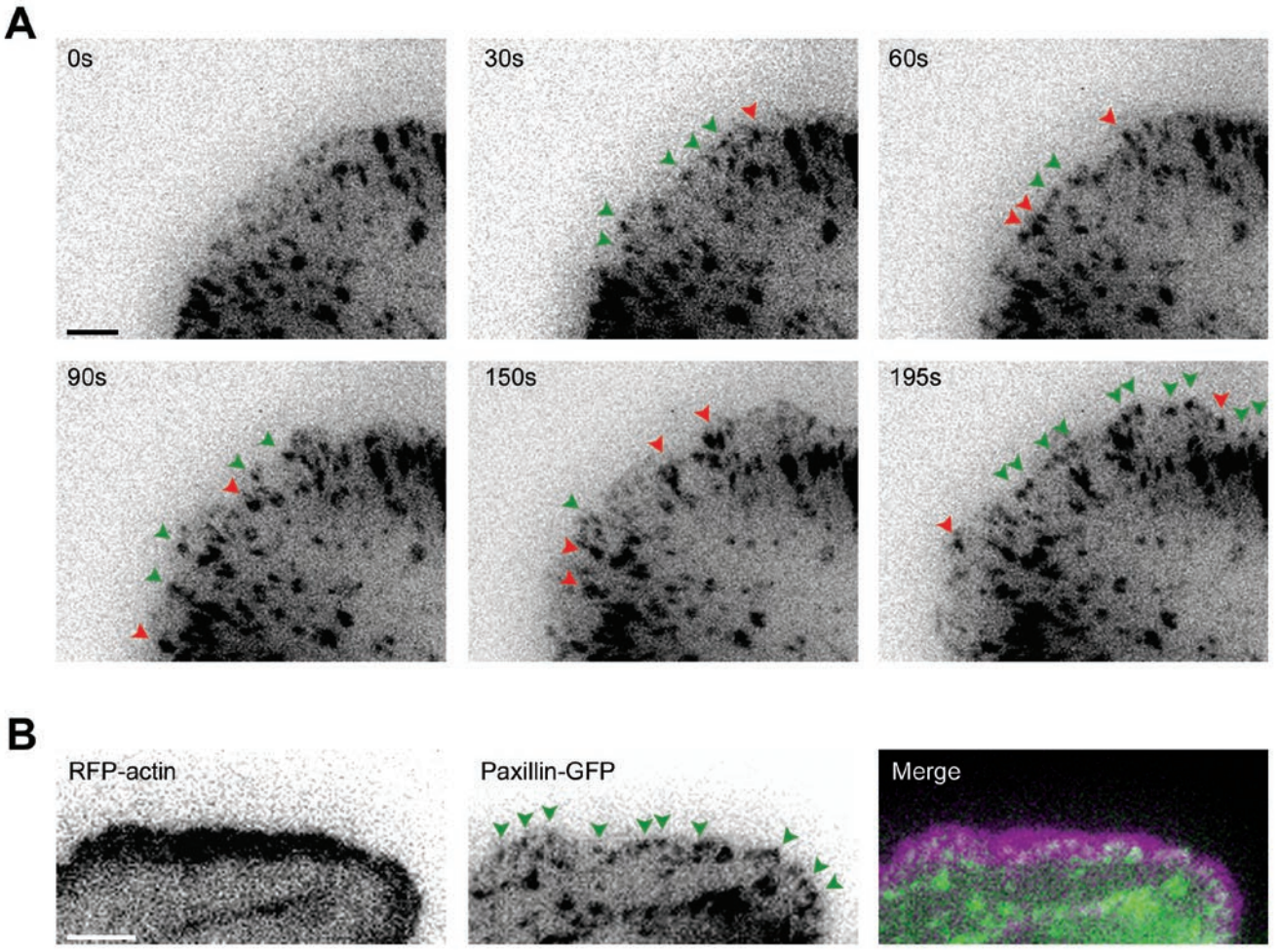

Figure S4 The rapid assembly of nascent adhesions in MEFs. TIRF time-lapse images of paxillin-GFP in MEFs show the rapid assembly (green arrows) of new nascent adhesions near the leading edge. Most nascent adhesions undergo immediate maturation and do not turnover (red arrows). Scale bar = 3 μm. Elapsed time is in seconds.TIRF images of GFP-actin (green) and paxillin-mOrange (magenta) show nascent adhesions (green arrows) forming in MEFs and residing exclusively in the lamellipodium. Scale bar = 3μm.

Supplementary Movies

Movie S1 Paxillin-containing nascent adhesions assemble and disassemble rapidly during protrusions. This movie corresponds to Fig. 1A. Images of paxillin-GFP collected every 1 sec using TIRF microscopy. Magenta and green arrows indicate representative assembling and disassembling adhesions, respectively. 10 frames/sec shown.

Movie S2 Nascent adhesions reside in the lamellipodium. This movie corresponds to Fig. 3A. Green indicates the lamellipodium marked by GFP-actin; magenta indicates nascent adhesions marked by paxillin-mOrange. Images collected every 3 sec using TIRF microscopy. 24 frames/sec shown.

Movie S3 Elongation of adhesions when a protrusion halts**.** This movie corresponds to Fig. 4A. Images of paxillin-GFP collected every 5 sec using TIRF microscopy. 24 frames/sec shown.

Movie S4 Long-term imaging of nascent adhesions showing formation, turnover and maturation**.** Images of paxillin-GFP collected every 5 sec using TIRF microscopy. 24 frames/sec shown.

Movie S5 Elongation of actin filaments when a protrusion halts. This movie corresponds to Fig. 4A. Images of GFP-actin collected every 1 sec using TIRF microscopy. 24 frames/sec shown.

Movie S6 Actin template elongates from maturing nascent adhesions. This movie corresponds to Fig. 4B. Merged images of GFP-actin (green) and paxillin-mOrange (magenta) collected every 3 sec using TIRF microscopy. 24 frames/sec shown.

Movie S7 MIIA links to actin templates distal to the initial α-actinin. Merged images of GFP-actin (green) and mCherry-MIIA (magenta) collected every 5 s using TIRF microscopy. 24 frames/sec shown.

Movie S8 Adhesion turnover and maturation are inhibited by α-actinin knockdown. This movie corresponds to Fig. 5D. Images of GFP-actin and paxillin-mOrange collected every 3 sec using TIRF microscopy. 24 frames/sec shown.

Movie S9 Rescue of MIIA-knockdowns with wild-type-MIIA or the high actin affinity, non-contractile mutant, N93K-MIIA**.** This movie corresponds to Figs. 6A-C. Images of paxillin-mOrange collected every 3 sec using TIRF microscopy. 24 frames/sec shown.

Movie S10 Rescue of the MIIA knockdown with the non-contractile MIIA mutant N93K and blebbistatin. This movie corresponds to Fig. 6D. Images of paxillin-mOrange collected every 3 sec using TIRF microscopy. 24 frames/sec shown.

Movie S11 Rescue of the α-actinin knockdown by the high actin affinity, non-contractile mutant N93K-MIIA or over expression of MIIA wild-type**.** This movie corresponds to Fig. 7A-C. Images of paxillin-mOrange collected every 3 sec using TIRF microscopy. 24 frames/sec shown.

Movie S12 Paxillin-containing nascent adhesions assemble and mature rapidly during protrusions in MEFs. This movie corresponds to Supplementary Fig. 4O. Images of paxillin-GFP collected every 3 sec using TIRF microscopy. 24 frames/sec shown.

Movie S13 Myosin II regulates the probability and rate of nascent adhesion maturation. Left, MIIA-deficient CHO.K1cell. This movie is from Vicente-Manzanares et al., J. Cell Biol. 176(5)573-580, Suppl. Movie 7; center, wild-type; right, overexpression of MIIA in a CHO.K1 cell. Images of paxillin-GFP were collected every 5 s using TIRF microscopy. 24 frames/ s are shown.

Supplementary information: A mathematical model of nascent adhesion formation in the lamellipodium

Model assumptions

The main model assumption is that adhesion precursors (small ligated integrins or integrin clusters) start assembling into adhesion complexes only after some actin based adhesion precursors bind to growing dendritic actin filaments. Comparison with the data (below) shows that this process of binding is relatively slow, taking ~ 10-20 sec. In other words, physical contact with an actin filament is required for adhesion complex to be stabilized and to start incorporating paxillin, vinculin and other adhesion molecules (adhesion molecules in these complexes come on and off very rapidly, with rates of the order ~ 1/sec, so they are in a quasi-steady equilibrium with the actin/adhesion precursor density). The rate of this process of actin-precursor assembly is proportional to the total length of the dendritic filaments not yet associated with the adhesion complexes. Further, we assume that the branching takes place near the leading edge, only on adhesions, where the branching points firmly anchored to the substratum, or in the vicinity of the adhesions, where the existent dendritic filaments are stabilized close to the substratum. We assume that after actin subunits hydrolize ATP, and cofilin binds to the filaments and disassembles them, the adhesion complexes (or major part of them) either dissociate from the substratum together with F-actin and diffuse away or, without binding to actin, effective affinity of the complexes to the integrins becomes very small.

The quantitative model is based on the following assumptions:

1. Arp2/3 complexes are activated and associate with the existent dendritic actin filaments in the finite zone at the leading edge of width *L*. Branching and capping take place within this zone with constant rates s_0 and γ, respectively.

2. We approximate sequential processes of hydrolysis on actin subunits within the filaments, cofilin binding and severing and/or depolymerization of F-actin by a lumped disassembly process with constant rate *h*.

3. The process of binding of the actin-based precursor complex and adhesion precursors to the dendritic filaments is limited by the length density of the filaments not yet associated with adhesions. Respective rate is *k*. These assumptions lead to the following mathematical model.

Mathematical model

We translated the assumptions into the system of three equations describing three densities – that of the barbed ends of the growing dendritic filaments, $b(x,t)$, of the length density (total length filament length per unit of distance) of F-actin, $f(x,t)$, and of the adhesion complexes, $a(x,t)$. The variables and parameters of the model are

summarized in the table, and the geometry is illustrated in Fig. 9. We track these densities in one dimension, in proximal-distal direction, and measure the distance rearward from the lamellipodial front. Therefore, relative to the front, the F-actin and adhesion densities are moving steadily away from the front with the rate of protrusion V, while the barbed ends are stationary relative to the front, as they grow forward with the protrusion rate. Note, that in the mathematical model we assume for simplicity that the dendritic actin is stationary relative to the substratum. In this case, the actin retrograde flow is relative to the leading edge, with the rate equal to the protrusion rate. In more general case, the lamellipodial actin network can recoil and slowly creep backward being pushed by the membrane resistance. In that general case, the retrograde flow terms in equation (2,3) below have to be proportional to the protrusion rate plus speed of the flow in the lab coordinate system. Similarly, the actin growth term in equation (2) would have to be pro-rated. Finally, the growing barbed ends that do not yet reach the membrane can, in principle, grow faster than the protrusion rate until they reach the membrane. For simplicity, we neglect all these effect. Simulations (not shown) suggest that those do not change the model result qualitatively, unless the slip of dendritic actin with respect to the substratum becomes comparable in magnitude to the protrusion rate. Future research will be needed to accurately measure respective rates and to correlate the data with the model.

The equations governing the densities' dynamics have the form:

$$\underbrace{\frac{db}{dt}}_{\substack{\text{rate of change}\\ \text{of barbed end}\\ \text{density}}} = \underbrace{s(x)}_{\substack{\text{branching}\\ \text{rate}}} - \underbrace{\gamma b}_{\substack{\text{capping}\\ \text{rate}}} \qquad (1)$$

$$\underbrace{\frac{\partial f}{\partial t}}_{\substack{\text{rate of change}\\ \text{of F-actin}\\ \text{density}}} = \underbrace{Vb(x)}_{\text{actin growth}} - \underbrace{hf}_{\substack{\text{actin}\\ \text{diasassembly}}} - \underbrace{V\frac{\partial f}{\partial x}}_{\substack{\text{retrograde flow}\\ \text{relative to the}\\ \text{leading edge}}} \qquad (2)$$

$$\underbrace{\frac{\partial a}{\partial t}}_{\substack{\text{rate of change}\\ \text{of adhesion}\\ \text{density}}} = \underbrace{k(f-a)}_{\substack{\text{rate of adhesion}\\ \text{assembly}}} - \underbrace{V\frac{\partial a}{\partial x}}_{\substack{\text{retrograde flow}\\ \text{relative to the}\\ \text{leading edge}}} \qquad (3)$$

Equations (2-3) are complemented by the boundary conditions $f(0,t) = a(0,t) = 0$: at the very leading edge, both F-actin length density, and adhesion density are equal to zero because of the effective retrograde removing both filaments and adhesion complexes from the boundary. Note, that we normalize the adhesion density so that in equilibrium it is equal to the F-actin density.

In the numerical simulation, we use the following spatial dependence of the branching rate:

$$s(x) = s_0\left(\frac{x^{\nu_1}}{x^{\nu_1}+l^{\nu_1}} - \frac{x^{\nu_2}}{x^{\nu_2}+L^{\nu_2}}\right) \approx s_0\begin{cases}1, & x < L\\ 0, & x > L\end{cases} \qquad (4)$$

In the simplified form, this rate is constant within the branching zone, and we use this simplification in the analytical solution derived below. Numerically though, to make the result more realistic, we smoothen the distribution at the front and rear of the branching

zone. In formula (4), l is the width of the region at the very front where the branching rate builds up (we used values $l = L$), and the exponents ν_1, ν_2 determine the sharpness of the branching zone boundaries. In the simulations, we used $\nu_1 = 2, \nu_2 = 4$; the results are not sensitive to the exact values of l, ν_1, ν_2.

Finally, equation (3) only describes the adhesion assembly within the branching zone. When the F-actin starts to disintegrate away from this zone, the adhesion density is simply proportional the remaining F-actin. Effectively, this means that the parameter k in this equation increases significantly away from the branching zone relative to its value in the zone.

Model variables	Meaning	Dimension	Value
t	time	min	
x	Distance from the front toward the rear	μm	
$b(x,t)$	Barbed end density	#/μm	
$f(x,t)$	Length density of actin filaments	μm / μm	
$a(x,t)$	Adhesion density	μm / μm	
Model parameters			
s_0	Branching rate	#/(μm×min)	Not specified, predictions do not depend on it
γ	Capping rate	1/min	Not specified, predictions do not depend on it
h	Actin disassembly rate	1/min	~ 0.5/min
k	Rate of actin-adhesion precursor association	1/min	~ 3-4/min
V	Protrusion rate	μm/min	~ 1.5 μm/min
L	Width of the branching zone	μm	~ 2 μm

Solution of the model equations

Stationary spatial distribution of the barbed ends near the leading edge follows easily from (1): $b = \frac{s(x)}{\gamma}$. Substituting this expression into (2), we obtain the equation for the stationary distribution of the F-actin: $\frac{df}{dx} + \frac{h}{V} f = \frac{s(x)}{\gamma}$. This first order linear ordinary differential equation with the boundary condition described above has the following analytical solution:

$$f(x)=\frac{1}{\gamma}\exp\left[-\frac{h}{V}x\right]\int_0^x \exp\left[\frac{h}{V}y\right]\times s(y)\times dy \qquad (5)$$

Similarly, from (3), the equation for the stationary distribution of the adhesion complexes has the form: $\frac{da}{dx}+\frac{k}{V}a=\frac{k}{V}f(x)$. The analytical solution of this equation is:

$$a(x)=\frac{k}{V}\exp\left[-\frac{k}{V}x\right]\int_0^x \exp\left[\frac{k}{V}y\right]\times f(y)\times dy \qquad (6)$$

In Fig. 8b, we used numerical integration and plotted the line profiles of the F-actin and adhesion densities predicted by formulae (5-6). In the plot, we used $\overline{x}=\frac{V}{h}$ as the distance scale, and $\overline{f}=\overline{a}=\frac{s_0 V}{h\gamma}$ as the densities' scale. In fact, we plot the temporal profiles, by simply using the fact that the transformation $x=V(t_0+t)$ connects the spatial coordinate and time in the steadily protruding lamellipod. The temporal profile can be obtained by substituting this transformation in place of *x* into (5-6).

The solutions are especially revealing if the simplified, step-like spatial profile of the branching rate is assumed. In this case, the integrals in (5-6) can be calculated explicitly, and the F-actin and adhesion distributions within the branching band can be predicted:

$$f(x)\approx\frac{s_0 V}{h\gamma}\left(1-\exp\left[-\frac{h}{V}x\right]\right),\ a(x)\approx\frac{s_0 V}{h\gamma}\left(1+\frac{h}{k-h}\exp\left[-\frac{k}{V}x\right]-\frac{k}{k-h}\exp\left[-\frac{h}{V}x\right]\right) \qquad (7)$$

Formula (7) says that close to the leading edge, when $x = V/k$, the F-actin density increases almost linearly: $f\approx\frac{s_0}{\gamma}x$. This means that in the temporal profile, the actin assembly rate would be $f\approx\frac{s_0}{\gamma}Vt$. Meanwhile, the adhesion density starts building up slowly: $a\sim x^2$ in the line profile, or $a\sim t^2$ in the temporal profile. Then, when initial lag phase is over, the adhesion density follows the F-actin density, which is especially clear in the limiting case $h = k$: $a\approx\frac{s_0}{\gamma}\left(x-\frac{V}{k}\right)$. This formula illustrates that in the line profile plot, the adhesion band front lags behind the actin band front by V/k. Similarly, in the temporal profile plot, adhesion band lags behind the actin one by the time $\tau\approx 1/k$ equal to the inverse rate of the assembly of the adhesion precursor onto the actin dendritic network.

Model predictions

The model correctly predicts the qualitative features of the observed line and temporal profiles of the F-actin and adhesion densities (see Fig. 8b): F-actin density builds up almost linearly at the leading edge, have a very short stability plateau, and then exponentially disassembles. Adhesion, after a lag, builds up almost precisely following

the actin profile. Then it either starts to disassemble, synchronously with the dendritic actin network, or has a short stability period before starting to disassemble.

Another semi-quantitative model prediction is that when the leading edge stalls, the barbed ends that still grow before abutting the cell membrane, accumulate at the leading edge, and so the F-actin density is finite immediately behind the leading edge. Also, the region of the actin disassembly $\sim V/h$ shrinks, so the actin band becomes narrower. The adhesion complexes can build up immediately behind the leading edge, where the actin density is now significant (without spatial gap between actin front and adhesion front, like in protruding edge). This prediction is also in agreement with the observations.

Yet another qualitative prediction that fits the data is that the rates of actin and adhesion assembly depend very little on fibronectin concentration, because the limiting rates are those of actin branching and of actin/adhesion precursor association independent of the ligation and/or integrin activation rates.

More importantly, the model makes a number of quantitative predictions, all of them agreeing to the data. First, the rate of the actin/adhesion disassembly, h, is independent of the protrusion rate. Second, the apparent assembly rate is predicted to be $s_0 V/\gamma$, so it has to increase as the protrusion rate grows.

Third, the model predicts that the time lag between actin and build up is constant, independent of the protrusion rate, in the temporal density profiles. In the line profiles, this lag is proportional to the protrusion rate. The constant time lag is $\tau \sim 15$ sec, while the spatial lag is $x \sim 0.3$ um, in agreement with the fact that at the observed protrusion rate, $V \sim 1.5$ μm/min, *x:* $V\tau$.

Finally, the average 'pause duration' for the adhesion complexes – time interval where their density is stabilized – can be explained as follows. The F-actin density increases linearly at the leading edge at first, and then is stabilized by the balance between branching and growth and disassembly. This stability period ends because the branching zone is finite, and behind it the disassembly ensues. The small actin density stability plateau is seen in the Fig. 8b. When this period is small, the lagging adhesion density does not have time to equilibrate with actin, and starts to decrease after a sharp peak, as is send in the example in the Fig. 8b. However, if the actin growth is over long before the branching zone is passed, the adhesion density has enough time to equilibrate with the F-actin, and the adhesion 'pauses' before it starts disassembling. The time from the beginning of actin assembly to the onset of the disassembly is L/V, the time of the actin build-up is $\sim \gamma / s_0 V$, and the adhesion lag time behind the actin, τ, is constant. Therefore, we predict that the pause duration for the adhesion complexes, $\left(\frac{L - \gamma / s_0}{V} - \tau \right)$, is inversely proportional to the protrusion rate. This prediction agrees with the data statistics.